Eur. J. Mech. B - Fluids 20 (2001) 25–46

S0997-7546(00)01105-5/FLA

The manipulated transitional backward-facing step flow: an experimental and direct numerical simulation investigation

Hans Wengle [a,*], André Huppertz [b], Günter Bärwolff [c], Gerd Janke [b]

[a] *Institut für Strömungsmechanik u. Aerodynamik, LRT/WE 7, Universität der Bundeswehr München, 85577 Neubiberg, Germany*
[b] *Hermann-Föttinger-Institut für Strömungsmechanik, Technische Universität Berlin, 10623 Berlin, Germany*
[c] *Fachbereich 3, Mathematik, Numerische Mathematik u. Funktionalanalysis, Technische Universität Berlin, 10623 Berlin, Germany*

(Received 15 May 1999; revised 1 February 2000; accepted 5 July 2000)

Abstract – Results from a joint experimental and direct numerical simulation (DNS) investigation are presented for the flow over a backward-facing step manipulated by low-amplitude time-periodic (harmonic) blowing/suction excitation through a narrow slot at the edge of the step. For a Reynolds number of $Re_h = 3000$ (based on step height, h, and inflow velocity, U_o) and for laminar inflow, a 33% reduction of the mean recirculation length (in comparison to the non-manipulated reference case) could be obtained with a forcing amplitude of the order of one per cent of U_o. Based on the momentum thickness, θ, of the incoming laminar boundary layer (at the edge of the step), the corresponding optimum Strouhal number is $St_\theta = f_{\mathrm{opt}}\theta/U_o = 0.012$. From the experimental data it can be concluded that, in our flow case, the optimum frequency, $f_{\mathrm{opt}} = 50$ Hz , was the most amplified frequency in the transition-to-turbulence process of the separated laminar shear layer. Detailed comparison of the experimental data with data from the numerical simulation shows that DNS and experimental data agree up to second-order statistics. The joint experimental and numerical investigations exhibit a complementary nature in the sense that, on the one hand, the main advantage of the experiment was the relative ease with which a wide range of forcing parameters could be tested and, on the other hand, DNS could provide spatio-temporal details of the flow which could not be so easily obtained in the experiment. © 2001 Éditions scientifiques et médicales Elsevier SAS

backward-facing step flow / time-periodic forcing / measurements and direct numerical simulation (DNS) / optimal frequency / control of mean re-attachment length

1. Introduction

The understanding of flow separation and re-attachment is important for the design of many engineering applications. On the one hand, the presence of recirculation and turbulence may help, e.g. to enhance mixing in a flow and, on the other hand, the presence of separated flow regimes may cause a loss of energy. So, there is a need for the improvement of fluid dynamic processes involving transitional or fully turbulent flows. It has been shown that the structure of turbulence may be manipulated to achieve a certain desired behaviour of the flow, such as drag reduction, minimization/maximization of mixing, or the reduction of separation. For this, a deeper understanding of the underlying dynamics of the basic structures in turbulent flows is required. Knowledge about the three-dimensional and time-dependent flow fields can be obtained from measurements in the real world of the laboratory or, thanks to the increased power of modern 'super'-computers, from results of numerical simulations of idealized flows.

There are two basic numerical simulation concepts available to calculate the three-dimensional and time-dependent structure of a turbulent flow (based on the solution of the Navier–Stokes equations). The Direct Numerical Simulation (DNS) resolves all the relevant scales in a turbulent flow, but its range of application is

* Correspondence and reprints.
E-mail address: hans.wengle@unibw-muenchen.de (H. Wengle)

limited to relatively small Reynolds numbers (often too small from a practical engineering point of view). Moin and Mahesh [1] illustrate the complementary nature of experiment and direct numerical simulation in turbulence research. Significant insight into the turbulence physics has been gained from DNS of certain idealized flows that cannot be easily attained in the laboratory. Large-Eddy Simulation (LES) delivers directly the spatial and temporal behaviour of at least the large-scale structures also for higher Reynolds number flows, and only the effects of the small-scale motions which cannot be resolved on a given computational mesh need to be modelled with a so-called sub-grid scale model. LES still requires further development concerning these sub-grid scale models and, in addition, improvements in modelling the flow regime close to rigid walls (wall function approach).

Among the geometries used for studies of separated flows, the most frequently selected one is the backward-facing step: the geometry is simple, the separation point is fixed at the step and the streamlines approaching the step are nearly parallel to the wall. There is only one major separation region with mean re-attachment at about six to eight step heights (for Reynolds numbers above 1000). After re-attachment the flow slowly relaxes toward an equilibrium turbulent boundary layer.

A review of research on turbulent flow re-attachment was given by Eaton and Johnston [2] and a more recent one by Adams and Johnston [3,4]. For turbulent boundary layer inflow, and a step height Reynolds number of 5100, a DNS is available from Le et al. [5], and a corresponding LES from Akselvoll and Moin [6]. Their results are compared with experimental data from Jovic and Driver [7]. Results from a LES by Delcayre [8] for this flow case ($Re = 5100$) are also compared with this experiment. Other experiments have been carried out by Itoh and Kasagi [9], for $Re = 5400$ and by Kasagi et al. [10], for $Re = 5500$. For turbulent flow over a step in open channel flow measured data are available from Nezu and Nakagawa [11], for a range of Reynolds numbers from $Re = 8000$ to $Re = 23000$. For turbulent boundary layer inflow, LES solutions for $Re = 46000$ are available from Kobayashi and Togashi [12]. For transitional inflow boundary layer, Yoo and Baik [13] presented experimental data for the redeveloping boundary layer after re-attachment in the backward-facing step flow ($Re = 40000$). For turbulent channel inflow, Friedrich and Arnal [14] compared their results for $Re = 155000$ with experimental data from Durst and Schmidt [15]. The case of laminar boundary layer inflow is of particular interest because the free shear layer undergoes transition to turbulence and, over a relatively long distance, this shear layer is dividing a turbulent separation zone below from a non-turbulent region above. Early experimental data is available from Sinha et al. [16], for $Re = 662$ up to $Re = 2648$. There is also some information on the onset of three-dimensionality and early transition from a DNS investigation of Kaiktis et al. [17] for $Re = 800$. LES solutions (at $Re = 38000$) are available from Neto et al. [18] for forced transition using as inflow a stationary mean velocity profile with superimposed white noise of amplitude $10^{-4}U_{\max}$.

Reviews on the management and control of laminar/turbulent flows were given by Bushnell and McGinley [19], Fiedler and Fernholz [20], Gad-el Hak [21], Lumley and Blossey [22], and a most recent collection of review articles by Gad-el Hak et al. [23]. Related to the topic of this paper are reports on more recent experimental work by Kiya et al. [24] and by Sigurdson [25] on a forced separation bubble on a blunt cylinder aligned coaxially with the free stream. The manipulation of the free shear layer after a backward-facing step was investigated by Hasan [26] for laminar separation ($Re = 11000$) and by Hasan and Khan [27] for transitional and turbulent boundary layer inflow ($Re = 15000$ and 30000). Experimental data for a manipulated fully turbulent backward-facing step flow ($Re = 12000$ to $Re = 33000$) was presented in Chun and Sung [28,29].

In this paper we report on an experimental and numerical simulation investigation of a backward-facing step flow, at $Re_h = 3000$ with laminar inflow, manipulated by low-amplitude time-periodic (harmonic) blowing/suction forcing at the edge of the step. One of the main objectives of this investigation is the reduction of the mean re-attachment length (defined as the location of zero wall-shear stress). This measure of the downstream extension of the mean separation zone depends in the natural (non-manipulated) situation on

many parameters, such as (a) the Reynolds number, Re_h, (b) the state of the flow at separation (laminar or turbulent), (c) the ratio of boundary layer thickness to step height (at the edge of the step), (d) the turbulence intensity in the free stream, and (e) the expansion ratio, ER, of the step configuration (defined as the ratio of the vertical dimension of the problem after and before the step). If we restrict ourselves to two-dimensional harmonic blowing/suction forcing at the edge of the step, the change of the re-attachment length depends on two additional parameters: the frequency and amplitude of these excitations. It is known from earlier work that an optimum frequency exists for a maximum reduction of the mean re-attachment length. Limited resources required us to restrict the number of parameters for a concurrent experimental and numerical investigation. Therefore, a Reynolds number $Re_h = U_o h/\nu = 3000$ (based on step height, h, and maximum inflow velocity at separation, U_o), a laminar boundary layer inflow with $\delta_{0.99}/h = 0.21$, a low turbulence intensity in the free stream of less than 0.2% , and an expansion ratio of $ER = 1.09$ have been chosen. For this Reynolds number a direct numerical solution (DNS) of the Navier–Stokes equation is possible, however still very expensive and therefore, the optimum forcing frequency for a maximum reduction of the mean re-attachment length had to be taken from the experiment. If the results of the experimental and numerical (DNS) investigation could later be used to verify correct sub-grid-scale modelling in a large-eddy simulation, then a series of (much cheaper) LES for such a search for an optimum parameter in other manipulated flows can be performed. A first step in this direction was already carried out by Orellano and Wengle [30] to investigate the optimum forcing frequency for turbulent boundary layer flow over a fence ($Re_h = 3000$). Both investigations presented in this paper run more or less in parallel but the final experimental data was actually available for a detailed comparison only after the second-order statistics had already been collected in the computations. Preliminary results from a pilot study of the DNS investigations presented in this paper were published by Bärwolff et al. [31] and preliminary results from the experimental investigations were presented by Huppertz and Janke [32].

The main objectives of this study are:

(a) to carry out experimental investigations and direct numerical simulations of the same backward-facing step flow with laminar inflow;

(b) to manipulate this flow by low-amplitude blowing/suction (generated by loudspeakers) through a narrow slot close to the edge of the step in order to obtain a shorter mean separation zone;

(c) to compare and discuss the data of these two investigations; and

(d) to study the dynamical processes which lead to a reduction of the re-attachment length.

In this paper we will present mainly results for the first-order and second-order statistics and only touch upon instantaneous flow events. In a separate paper we will discuss the turbulent flow structure in more detail. In the following section 2 we present the experimental set-up and the measurement technique used in the experiment. The numerical method and the computing strategy used in this study is described in section 3. We compare and discuss the experimental and computational results in section 4, followed by our conclusions in section 5.

2. Experimental set-up and measurement techniques

2.1. Experimental arrangement

The experiments were performed at the Hermann-Föttinger Institute (Technical University of Berlin) in a low-speed open-circuit wind tunnel (see *figure 1*). It was driven by a centrifugal blower attached through a wide-angle diffusor with a circular settling chamber. A number of screens prevented flow separation in the wide-angle diffusor. The settling chamber was equipped with a filter mat followed by a perforated plate (open area ratio: 64%). This arrangement has proven to provide very uniform flow conditions in the test section (see

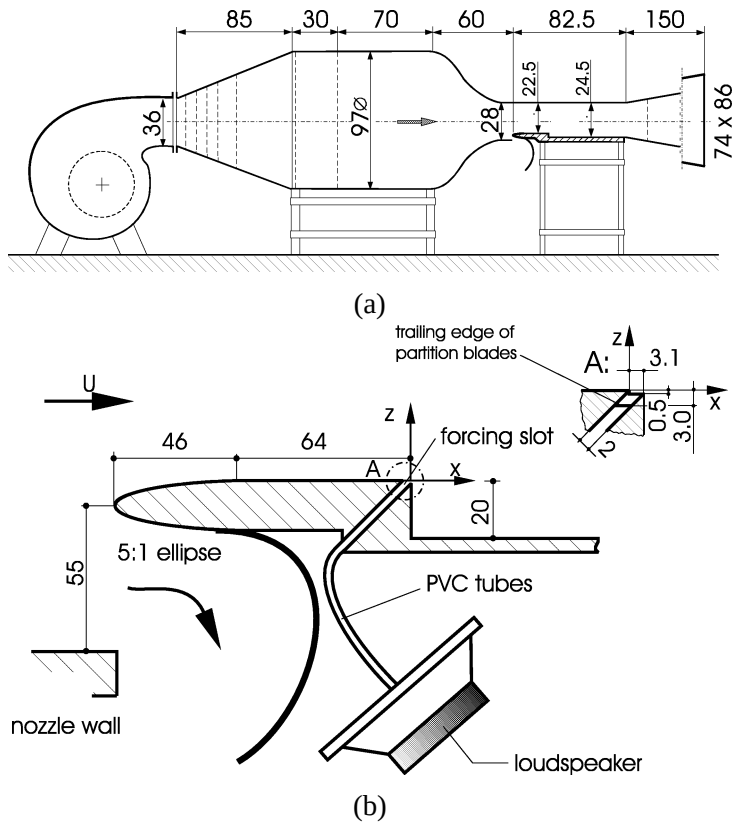

Figure 1. Experimental set-up: low speed wind tunnel (above, measures in cm) and test section with backward-facing step model (below, measures in mm).

Dengel [33]). The nozzle had a 6.25 contraction ratio, a circular inlet and a rectangular outlet. The test section had a rectangular cross section of 400 mm $\times$ 245 mm and a length of 825 mm. The top and the side-walls of the test section were made of plexiglass to allow Laser-Doppler measurements and flow visualizations. The test section floor was a flint-glass plate blackened on its back side. This is especially suitable for oil-film interferometry (see Janke [34]), and also allows low-noise near-wall Laser-Doppler measurements. The test section was followed by a diffusor to minimize outlet-fluctuations which might be fed back into the test section [35].

The backward-facing-step model was fixed in the inlet of the test section (*figure 1*). It consisted of a 5:1 elliptical nose followed by a straight-wall section, the step and an off-center horizontal splitter plate. The step height could be varied between 0 and 40 mm. Except for the experiments discussed in section 2.4 the step height was $h = 20$ mm, the aspect ratio was 20 and the expansion ratio was $ER = 1.09$. The nose tip was raised 55 mm above the bottom side of the nozzle exit so that the nozzle boundary layer was blown out. In order to obtain well defined starting conditions for the newly developing laminar boundary layer the stagnation point was fixed at the upper side of the elliptical nose with the help of an additional resistance in the outlet diffusor. All experiments were conducted at a reference velocity of $U_o = 2.2$ m/s (the maximum velocity at separation). The free-stream turbulence intensity in the test section was less than 0.2%.

Figure 2 shows excellent lateral homogenity of the mean separating boundary layer profiles: it is a 2D laminar (Blasius-like) boundary layer profile with a momentum thickness $\theta = 0.535$ mm ($\theta/h = 0.027$) and a boundary layer thickness $\delta_{0.99} = 4.2$ mm ($\delta_{0.99}/h = 0.21$). The flow displacement around the nose causes an overshoot

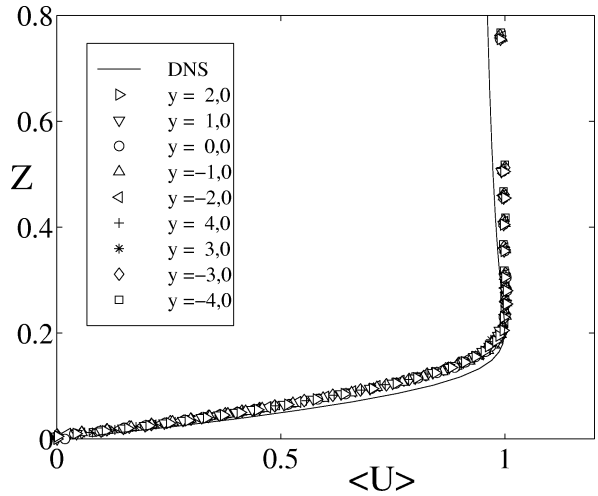

Figure 2. Flow condition at the edge of the step ($x/h = 0$): measured mean streamwise velocity profiles at different lateral locations and comparison with DNS result; (symbols) experiment, (full line) DNS.

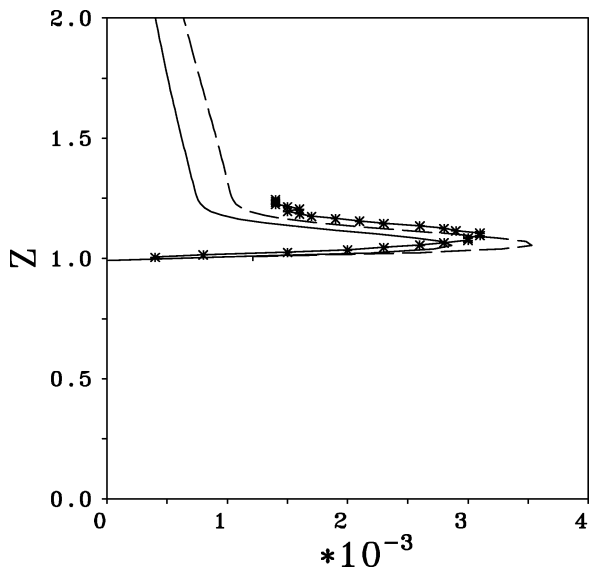

Figure 3. Vertical u-rms profiles close to the step ($x/h = -0.05$) for the non-manipulated case: (symbols) experiment, hot-wire measurements, (full line) DNS using a 4th-order method, (dashed line) DNS using a 2nd-order method.

near the wall. The u-rms values of the stream-wise fluctuations at separation from hot-wire measurements are presented in *figure 3*.

2.2. Measurement techniques

Except for a few measurements with a single hot-wire in the free stream (where low turbulence levels had to be resolved), the bulk of the velocity measurements was conducted with a commercial two-component LDA-system (Dantec fiber flow optics and burst spectrum analyzers 57N10). It was operated in the continuous mode measuring coincident velocities only. The averaging time was 30 seconds, a typical burst rate in the shear

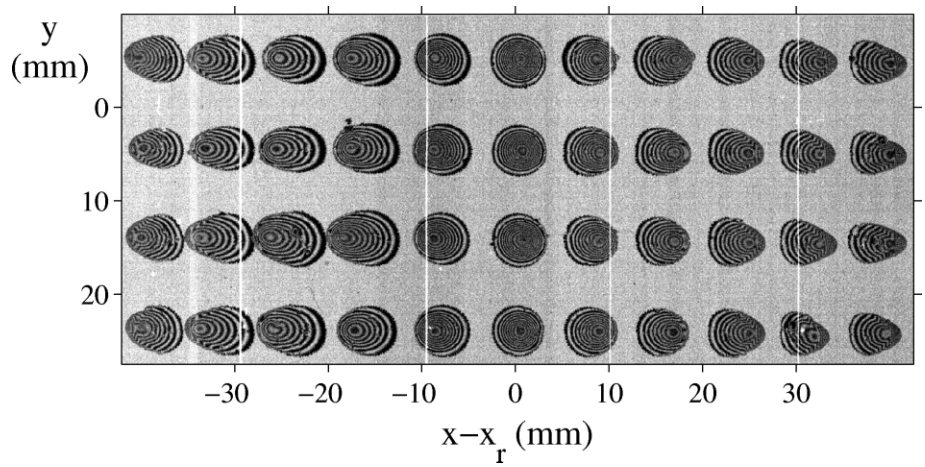

Figure 4. Determination of mean re-attachment length from an array of oil droplets on the test section floor (after a 15 min run).

layer was 1.5 kHz. Oil-film interferometry was employed to measure the mean re-attachment location and the wall-shear stress. *Figure 4* shows a picture (taken with a hand-held scanner) of an array of oil droplets on the test section floor after a 15 minutes wind-tunnel run. The interference fringes present contours of the film thickness. The innermost ring of each drop has moved into the direction of the flow. The re-attachment line can be determined with an accuracy of about ± 3 mm from this plot. No other method is known to us which is as sensitive and as easy to use at these very low test speeds. Skin-friction measurements were also done with oil-film interferometry, and the method is described in detail in Janke [34]. The measured data presented in section 4.3 show excellent agreement with the DNS data. Wall pressure (of the order of only 3 Pa) was measured with a high sensitive capacitance pressure transducer (MKS Baratron 120 AD).

2.3. Forcing technique

A forcing array was located right downstream of the separation edge (see *figure 1*) at the location of maximum receptivity for periodic perturbations [36]. It consisted of a lateral slot partitioned by 0.1 mm thin blades into 105 small square channels (cross section 2 mm $\times$ 2 mm). The blades ended 3 mm below the exit (see detail in *figure 1*). The blade wakes were not detectable at the outlet with hot-wire scans and therefore a truly two-dimensional forcing could be realized. The forcing slot was inclined at 45° and the partitioned channels were connected via PVC tubes of equal length (diameter 1.6 mm, length 200 mm) to four loudspeakers. The equal length of the tubes ensured that the phase of the perturbation at the outlet of the holes was the same across the array width. The loudspeakers were driven by power amplifiers. A PC (CPU M68030) with a 12 bit D/A converter served as a multi-channel arbitrary-signal generator. With this equipment a wide variety of forcing modes could be tested, including single-frequency and multi-frequency forcing, span-wise uniform and span-wise non-uniform forcing at small and high amplitudes. For the joint project, presented in this paper, a single-frequency span-wise uniform excitation with small amplitudes was taken. The forcing amplitude, $A \equiv v_f/U_o \approx 4\%$, was determined from phase-averaged LDV measurement of the stream-wise and wall-normal velocity components of v_f immediately above the slot. *Figure 5* shows typical profiles of the rms values of the u velocity component for the forced step flow ($f = 50$ Hz) close to the edge of the step ($x/h = 0.09$), taken at different lateral positions and indicating satisfactory lateral uniformity of the forcing.

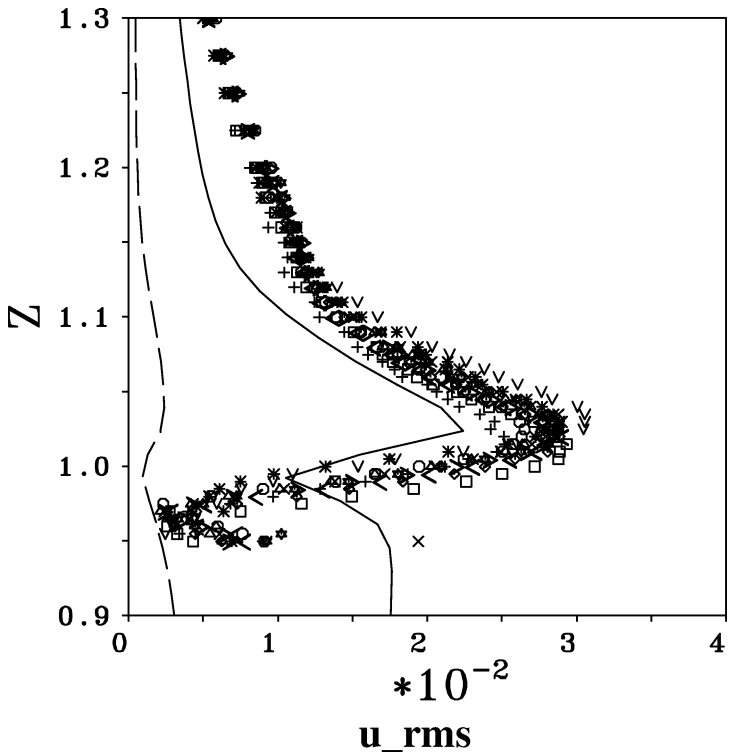

Figure 5. Vertical u-rms profiles close to the edge of the step ($x/h = 0.09$) for the manipulated flow case. Lateral homogeneity of measured u-rms profiles (different symbols for different lateral positions, see *figure 2*). Comparison with DNS results for different amplitudes of the disturbance: (dashed line) $A = 10^{-4}$, (full line) $A = 10^{-2}$.

2.4. Global forcing effects

In order to gather some information on the scaling of the optimum forcing frequency, two different flow configurations with $Re_h = 1480$ and 3000 were forced in a frequency range between 0 and 400 Hz with a constant forcing amplitude of about 4%. The Reynolds number was varied by changing the step height ($h = 10$ and 20 mm), while the state of the separating boundary layer ($Re_\theta \approx 83$) was kept constant. *Table I* contains the parameters of the two flow configurations together with the resultung re-attachment lengths x_{ro}/h for the unforced flows. *Figure 6* shows that for both step heights similar curves are observed for the dependence of the re-attachment length on the forcing frequency. In both cases, the shortest separation bubble occurs in the vicinity of 40 Hz. Thus, in our flow case the most effective forcing frequency does not scale with the step height as suggested by Sigurdsson [25]. The shortest separation bubble occurs slightly below the most amplified frequency (50 Hz) of the separated shear layer corresponding to a Strouhal number $St_\theta = f_{\text{opt}}\theta/U_{\text{ref}} = 0.012$. This indicates that the forcing frequency scales with the momentum thickness of the shear layer as shown by Hasan [26], at least for a small ratio of momentum thickness to step height ($\theta/h \ll 1.0$). The instability

Table I. Parameters of the unforced flow configurations.

h [mm]	Re_h	Re_θ	θ [mm]	θ/h	ER	x_{ro}/h
10	1480	83	0.566	0.0566	1.042	11.3
20	3000	82	0.532	0.0266	1.088	6.4

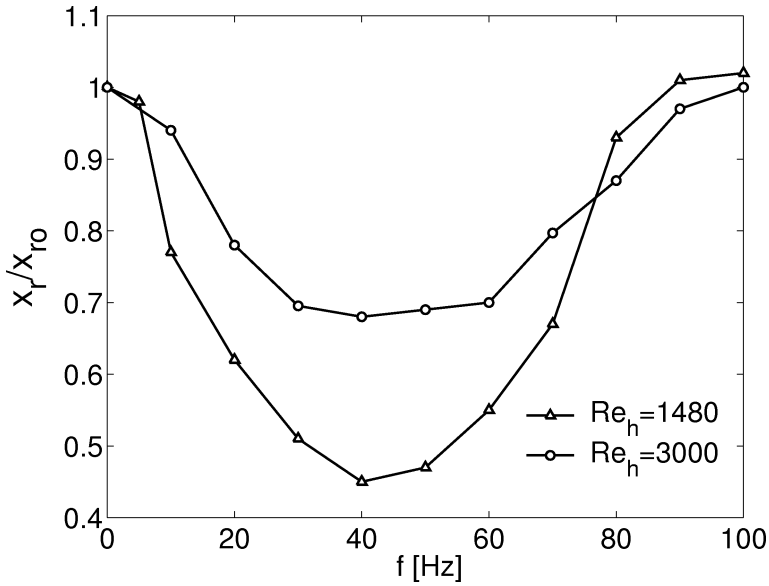

Figure 6. Mean re-attachment length x_r/x_{ro} versus forcing frequency, at two different Reynolds numbers.

studies of Michalke et al. [37] and Dovgal et al. [38] also demonstrated that the shear layer of the step flow is dominated by a Kelvin–Helmholtz type instability. In addition, for forced turbulent boundary layer flow over a backward-facing step, the experimental data of Chun and Sung [28,29] also show a maximum reduction of the mean re-attachment length at the same Strouhal number, $St_\theta = 0.01$, for the much higher Reynolds numbers $Re_h = 12000$, 23000 and 33000 (all cases with $\theta/h \approx 0.04$).

3. Numerical simulation

3.1. Solution strategy and numerical solution method

For a direct numerical simulation (DNS) the conservation equations for mass and momentum must be solved without any additional assumptions or modelling related to the effects of the turbulent motion; i.e. the original Navier–Stokes equations must be discretized in space and time such that all the relevant scales in a turbulent flow are resolved. For example, referring to spatial scales, the size of the computational domain must be large enough to accommodate the largest turbulent scales (which is determined by the typical scale of the apparatus), and the grid spacing must be sufficiently small to enable a resolution of the order of the dissipation length scale $\eta = (\nu^3/\varepsilon)^{1/4}$. Here, ν is the kinematic viscosity of the fluid and ε is the dissipation rate in the flow field. Less stringent estimations consider, for example, two-point correlations and (one-dimensional) energy spectra to judge whether adequate resolution can be achieved.

The Navier–Stokes equations for an incompressible fluid are solved numerically on a staggered grid using second-order finite-differencing in time and space (explicit leapfrog for time discretization, central differencing for convection and time-lagged diffusion terms). The problem of pressure-velocity coupling is solved iteratively by a pressure (and velocity) correction method, requiring the dimensionless divergence to be below 10^{-3} after every time step at all grid points.

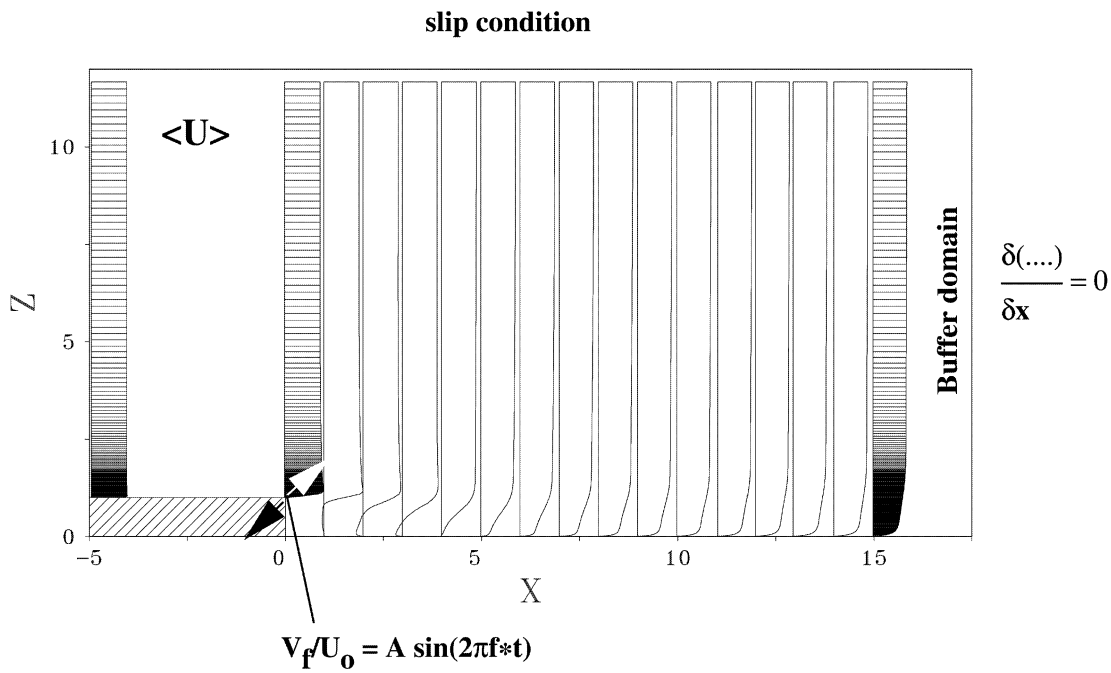

Figure 7. Computational domain and boundary conditions.

The direct results from a DNS are the time-dependent and three-dimensional velocity and pressure fields. After an initial transient phase of the calculation (not used for collecting samples for the statistics) the mean fields have been obtained by averaging samples in time and by making use of spatial averaging in the homogeneous lateral direction of the flow problem. As soon as the mean fields have reached stable (i.e. time-independent) values, the fluctuating fields can be evaluated. This was the case after about 220 reference times, $T_{\text{ref}} = U_o/h$. Then samples for the evaluation of the second-order statistics have been collected over additional 210 reference times.

3.2. Flow configuration, computational grid, and boundary conditions

The flow configuration selected is a backward facing step (see *figure 7*) with an expansion ratio of $ER = 1.09$. If all length scales are normalized with the step height, h, the dimensions of the computational domain are $(L_x, L_y, L_z) = (22.92, 6.0, 11.76)$ including an entry length of 5 reference lengths. Here, x is the main flow direction, y is the lateral direction, z is the vertical direction, and $x/h = 0$ corresponds to the position of the step. (Note that in *figure 11* and the following figures not the whole computational domain is visible).

The length of the entry section was sufficiently long that, starting from an uniform velocity profile at the inlet section (at $x/h = -5.0$), at the edge of the step ($x/h = 0$) a Blasius profile is developed with a boundary layer thickness of $\delta/h = 0.2$ (experiment: $\delta/h = 0.21$) and a momentum thickness of $\theta/h = 0.025$ (experiment: $\theta/h = 0.027$). This procedure also produced an overshoot of the mean velocity profile at the edge of the step as observed in the experiment, see *figure 2*. In addition, stream-wise velocity fluctuations developed and, immediately before the step ($x/h = -0.05$), the maximum of the u-rms values reached a magnitude of $3.0 \cdot 10^{-3}$ showing satisfying agreement of second-order and fourth-order solutions with the hot-wire measurements (see *figure 3*).

To resolve the relevant scales of the flow we used $(N_x, N_y, N_z) = (512, 128, 192)$ grid points in the stream-wise (x), the lateral (y), and the vertical (z) direction, i.e. about 12.6 million grid points. At the inlet section, the stream-wise grid spacing starts with a value of $\Delta X = \Delta x/h = 0.1$ which then slowly decreases to $\Delta X = 0.04$ at the edge of the step (at $X = x/h = 0.0$) and then remains constant throughout the computational domain. In the vertical direction, the grid spacing is constant with a value of $\Delta Z = 0.01563$ from $Z = 0.0$ to $Z = 1.5$, and then slowly increases to $\Delta Z = 0.18$ at $Z = 11.76$. In the lateral direction, we used an equidistant grid spacing of $\Delta Y = 0.046875$. Measured in units of the viscous length (using the wall-shear velocity $u_\tau = 0.055U_o$ from $X = 15.0$) the distance of the first grid point for the stream-wise velocity component (on the staggered grid) to the bottom wall is about $(\Delta Z^+/2) = 1.1$, the lateral resolution is about $\Delta Y^+ = 7.0$, and in the longitudinal direction the resolution is about $\Delta X^+ = 6.0$. From an a posteriori evaluation of the local (dimensionless) dissipation rate, ε, the Kolmogorov dissipation length scale, $\eta = (\nu^3/\varepsilon)^{1/4}$, could be estimated using the maximum value of ε in the flow field ($\varepsilon_{\max} \approx 0.04$). Measured in units of η the spatial resolution in this investigation was $(\Delta X_\eta, \Delta Y_\eta, \Delta Z_\eta) = (7.2\eta, 8.5\eta, 2.8\eta)$.

A no-slip boundary condition was used along the lower wall (with the step), and a slip condition was used along the upper boundary of the computational domain. Periodic boundary conditions were assumed in the lateral direction and, for the results presented here, normal gradients of flow variables have been set to zero at the outflow cross section and, in addition, a buffer section of length $2.7h$ has been added (at $x/h = 15.0$) to the original total length of the computational domain to avoid possible upstream distortions of the flow by this simple outflow boundary condition.

In the experiment the flow is manipulated by harmonic blowing/suction through a cross-wind slot (inclined at 45°) at the edge of the step (see *figure 1* and *figure 7*). This manipulation was implemented via time dependent boundary conditions for the horizontal (u) and vertical (w) velocity components on two neighbouring rows of grid points close to the edge of the step. The two forcing velocity components varied in time as $v_f/U_o = A \cdot \sin(2\pi f t)$, with frequency f and (dimensionless) amplitude A as the two main parameters of the forcing.

3.3. Choice of forcing frequency and amplitude

Before starting the numerical simulations it has been known from preliminary experimental investigations that an optimum forcing frequency in the range between 40 Hz and 60 Hz would lead to a maximum reduction in the mean recirculation length (see *figure 6*). A forcing frequency of $f = 50$ Hz, together with the reference velocity of $U_o = 2.2$ m/s and the reference length $h = 20$ mm from the experiment, corresponds to a Strouhal number $St_h = 0.45$ to be realized in the numerical simulation.

The selection of a forcing amplitude corresponding to the experiment was more difficult. After having carried out a series of simulations using three different amplitudes ($A = 10^{-5}, 10^{-4}, 10^{-2}$) we could compare the results for the u-rms profiles close to the edge of the step with (the meanwhile available) measurements at the same location. From these measured data (see *figure 5*) we found that an amplitude of $A = 10^{-2}$ was closest to the results of the experiments. Therefore, results from these two corresponding cases (experiment and DNS) for the manipulated flow are compared in this paper.

4. Comparison of experimental and numerical results

Note that in the following all the variables are presented in dimensionless form, i.e. the velocities and the velocity correlations are made dimensionless with the reference velocity, U_o, lengths are made dimensionless with the step height, h, and vorticity is made dimensionless with U_o/h.

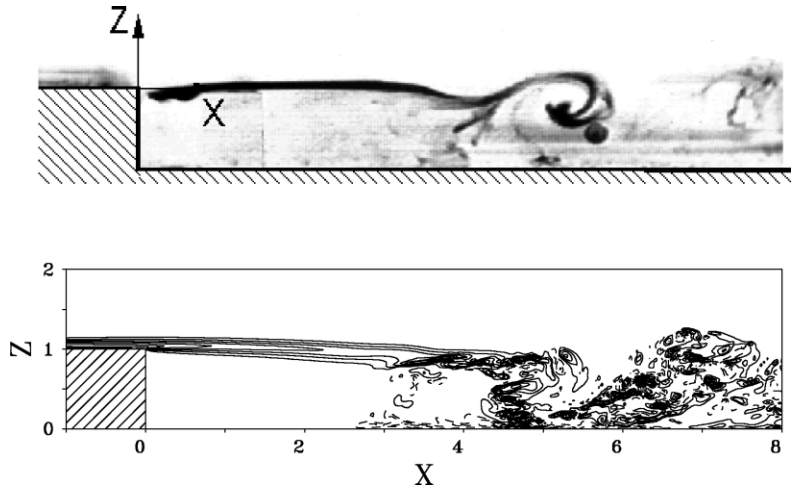

Figure 8. Flow characterization: above: photograph of smoke visualization in the unforced experiment; below: instantaneous iso-lines of the lateral vorticity ω_y from the DNS.

4.1. General flow characterization

Figure 8 shows a smoke visualization (above) and contours of lateral vorticity (below) of the unforced flow in order to give a general impression of the different regions in the flow and the different features of the flow. Close to the step, the separated flow regime is characterized by an initial laminar shear layer (about three step heights long) bounding a 'dead water' region of little turbulent activity. In the unstable shear layer, disturbances from below are amplified and finally roll up into two-dimensional vortices. Vortex pairing and the onset of three-dimensional vortices follow. Within a short interval the stream-wise and wall-normal vorticity components grow to the same magnitude as the lateral vorticity component. The entrainment of fluid creates a recirculation domain with strong turbulent activity before re-attachment (at about 6.5 step heights).

4.2. Mean wall pressure coefficient

The mean wall pressure difference normalized by $0.5\rho {U_o}^2$, $C_p = 2(\langle p \rangle - P_{\text{ref}})/(\rho {U_o}^2)$, is shown in *figure 9*. For convenience we selected the downstream wall pressure at $x/h = 15$ as the reference pressure, P_{ref}. Comparing the DNS result with the experimental data it can be seen that the pressure drop behind the flow obstacle is stronger in the numerical simulation, in particular for the manipulated flow case. Forcing shortens the separation bubble and thus shifts the pressure rise towards the step. Forcing also reduces the base pressure which is due to an increase of the streamline contraction right above the edge of the step.

4.3. Mean wall-skin friction coefficient

The mean wall-shear stress normalized by the maximum inlet velocity, $C_f = 2\tau_w/(\rho {U_o}^2)$, is shown in *figure 10*. The location of zero wall-stress determines the mean re-attachment length, x_r/h. For the compared flow cases there is very good agreement between numerical simulation and experiment. Both flow cases exhibit large peaks of negative skin friction coefficients ($C_f \approx -7.0 \cdot 10^{-3}$) in the recirculation zone. This is more than twice the corresponding peak value in the case of turbulent boundary layer inflow (Le et al. [5]). Also included in *figure 10* is the skin-friction distribution of another DNS to show the effect of changing the forcing

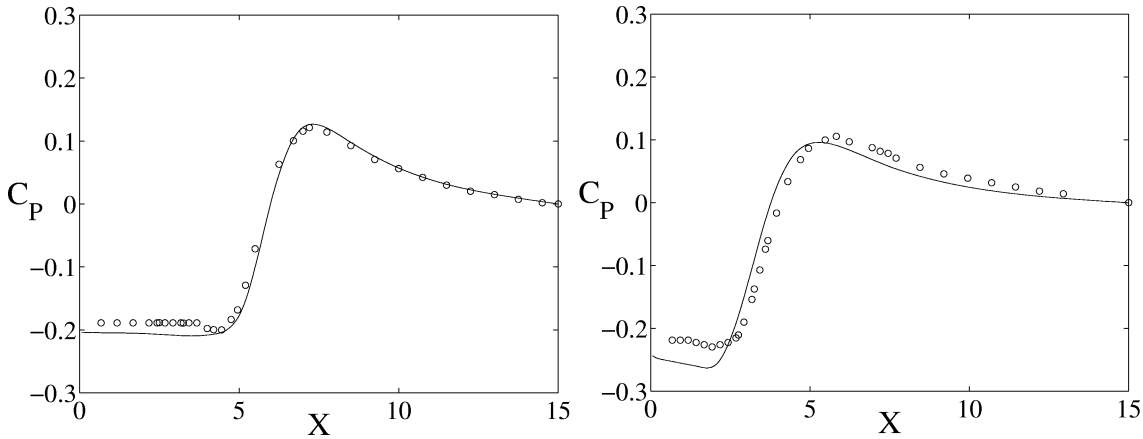

Figure 9. Horizontal profiles of mean wall pressure coefficient $C_p = 2(\langle p\rangle - P_{\text{ref}})/(\rho {U_o}^2)$ for the (non-manipulated) reference case (left) and for the manipulated case (right), for both cases: reference pressure $P_{\text{ref}} = \langle p\rangle$ (at $X = 15.0$).

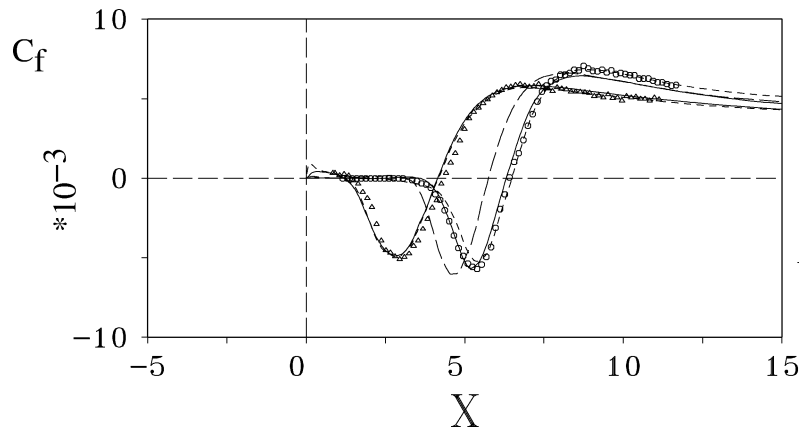

Figure 10. Horizontal profiles of mean wall-skin friction coefficient $C_f = 2\tau_w/(\rho {U_o}^2)$. experimental data: (open circles) $A = 0.0$, (triangles) $A = 10^{-2}$, DNS: (short dashes) 2nd-order method, (full lines) 4th-order (compact) method, (long dashes) $A = 10^{-4}$.

amplitude from $A = 0.0$ to $A = 10^{-4}$. Increased forcing does not change the general shape of the distributions. It just moves the re-attachment line ($C_f = 0$) closer to the step.

4.4. Mean re-attachment length

A characteristic measure of the size of the recirculation region is the mean re-attachment length, x_r/h. In the preliminary numerical simulations of Bärwolff et al. [31] using a smaller vertical extent of the computational domain ($Z_{\max} = 6.0$, i.e. $ER = 1.2$), $x_r/h = 7.4$ was calculated. Using the same grid but adding additional grid points to realize an extended vertical computational domain ($Z_{\max} = 11.76$, $ER = 1.09$) leads to much better agreement with the experiment. For the non-manipulated flow case this length was determined from the experiment to $x_r/h = 6.4$ and from the DNS to $x_r/h = 6.5$. According to the compilation of experimental data given by Adams and Johnston [3,4], x_r/h is indeed dependent on ER (around the Reynolds number considered here). In the manipulated flow case, the mean re-attachment length was shortened to $x_r/h = 4.4$ (experiment)

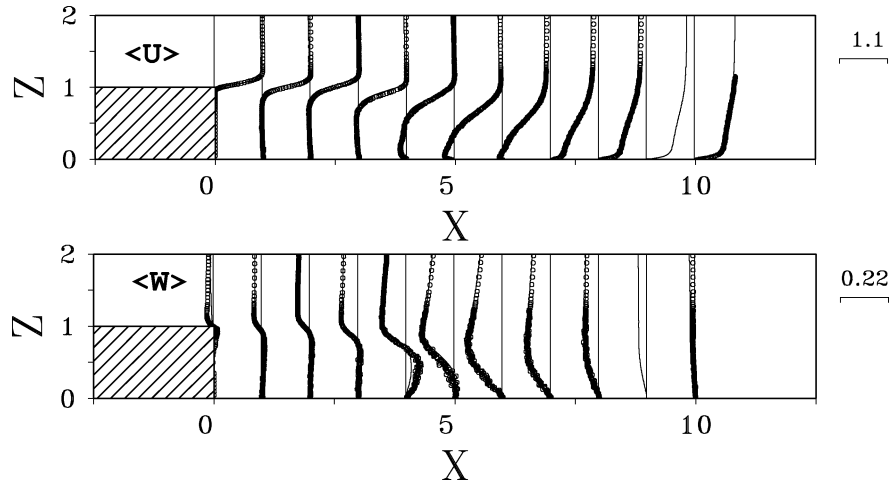

Figure 11. Vertical profiles of mean longitudinal velocity $\langle U \rangle$ for the non-manipulated reference case at different positions X, (open circles) experiment, (full line) DNS.

and to $x_r/h = 4.2$ (DNS), respectively. This means that the mean reverse-flow distance was reduced by 33% using time-periodic 2D disturbances with a low-amplitude (of the order of 1% of U_o).

4.5. Mean velocity profiles

A comparison of experimental and DNS data for the mean stream-wise velocity $\langle U \rangle$ and the mean vertical velocity $\langle W \rangle$ is presented in *figure 11* for the non-manipulated reference case. In general, the mean vertical velocity component $\langle W \rangle$ is about one order of magnitude smaller than the mean stream-wise velocity component $\langle U \rangle$, with significantly increased negative values of $\langle W \rangle$ in the re-attachment zone. The maximum back-flow is about 20% of the free-stream velocity (and it is not increased by forcing). In both flow cases, the mean stream-wise velocity component, $\langle U \rangle$, is still far from having recovered to a fully developed turbulent boundary layer profile close to the exit plane ($x/h = 15.0$).

4.6. Reynolds stresses

Examples of vertical profiles from the second-order statistics are given in *figures 12* and *13* for the non-manipulated flow case and in *figures 14* and *15* for the manipulated flow case. Inside the reverse-flow region the DNS values for the second-order statistics are smaller than the experimental data for the non-manipulated case and larger than the experimental data for the manipulated case. The qualitative behaviour of the DNS result is in agreement with the experiment, even in the low-turbulence region close to the step. The quantitative differences could be caused by differences in the unforced transition (in the non-manipulated reference case) and by the differences in the inflow conditions. However, note that at $X = 2.0$ the values of $\langle uu \rangle$ and $\langle uw \rangle$ are of the order of 10^{-3} and 10^{-4}, respectively, and the limitations also of the LDA measurements become obvious. In comparison with the fully turbulent backward-facing step flow of Le et al. [5] the fluctuations in the transitional case are significantly more intense. Le et al. report a maximum shear stress of $\langle uw \rangle = -0.011$. In the present investigation the maximum shear stress is $\langle uw \rangle = -0.022$. This has also been observed in other transitional flows, for instance in free shear layers (see Bradshaw [39]).

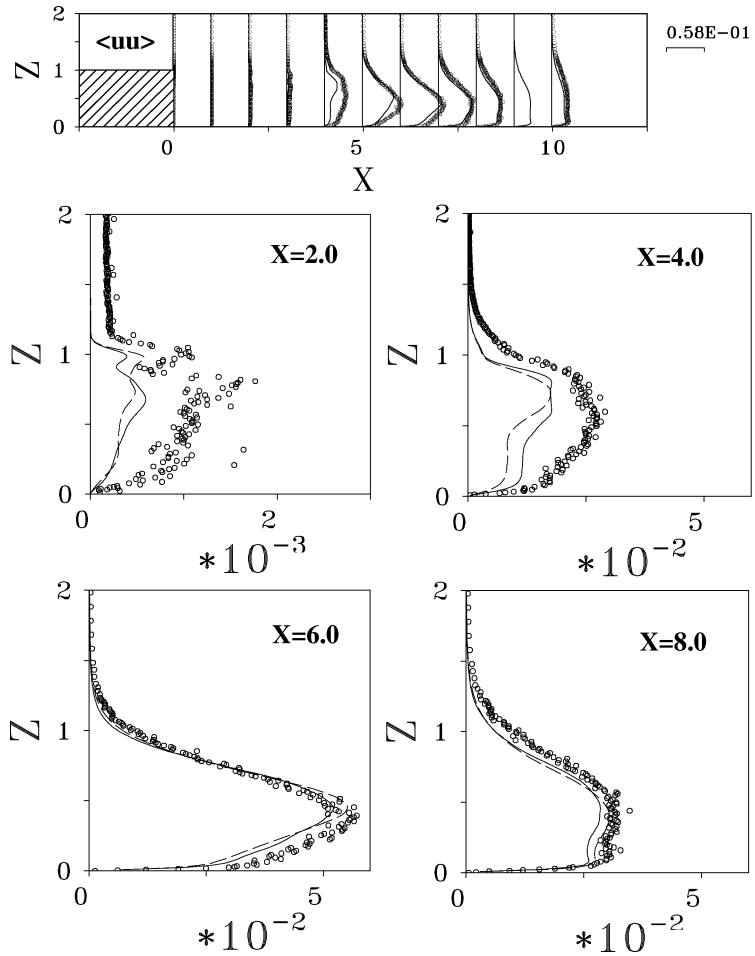

Figure 12. Vertical profiles of longitudinal normal stress $\langle uu \rangle$ for the (non-manipulated) reference case at different positions X: (open circles) experiment, (dashed line) 2nd-order method, (full line) 4th-order (compact) method.

4.7. Re-attachment zone

Additional DNS profiles of the normal Reynolds stresses in the lateral direction, $\langle vv \rangle$, and of the turbulent kinetic energy, k, are presented in *figure 14* for the manipulated flow case (experimental data was not available). As in all cases with re-attaching shear layers, large lateral fluctuations contribute significantly to the turbulent energy in the re-attachment zone. *Figure 16* presents a vector plot of the instantaneous flow field in a horizontal plane close to the bottom wall. It shows local stagnation regions with velocity vectors toward the wall inside these patches and away from the wall (in a more or less ring-like fashion) around these regions. Strong horizontal velocity fluctuations are created close to the wall by the splashing down of the flow onto the bottom plate. The effects of these events are mainly visible upstream of the instantaneous re-attachment line. If hydrogen bubbles are released in water, or if smoke is released in air into the reverse flow region upstream of the re-attachment line, the admixtures are turned aside by these local stagnation patches (see *figure 16*), called ‘black holes’ in [40].

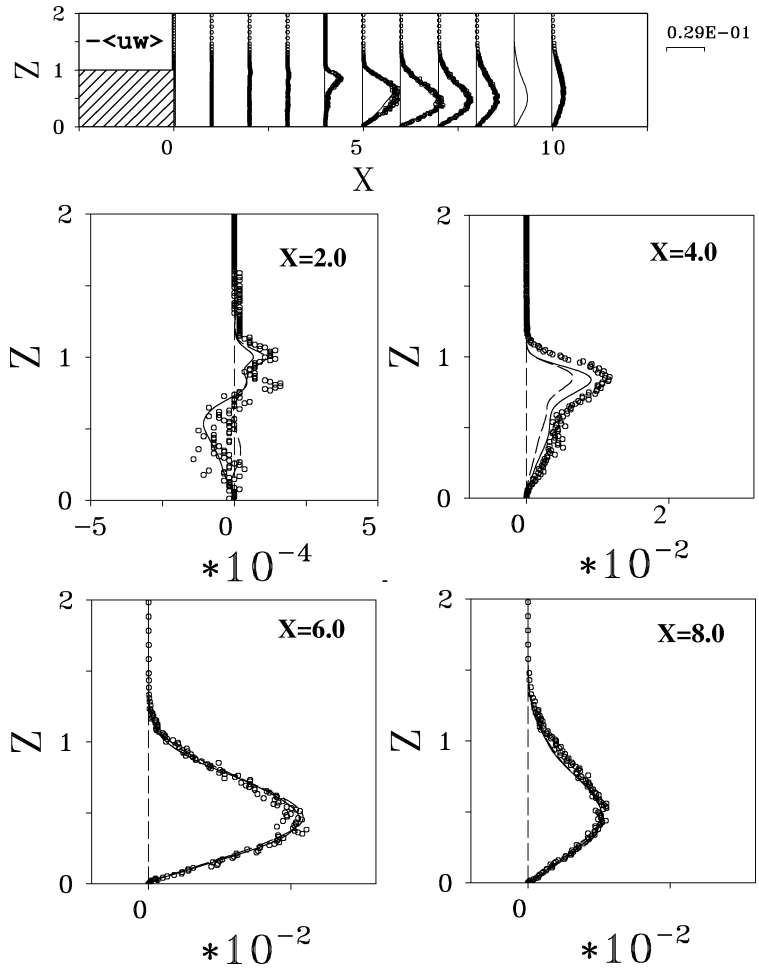

Figure 13. Vertical profiles of shear stress $\langle uw \rangle$ for the non-manipulated reference case at different positions X: (open circles) experiment, (dashed line) 2nd-order method, (full line) 4th-order (compact) method.

4.8. Transition to turbulence

In the experiment the separating boundary layer was laminar and the free-stream turbulence intensity was less than 0.2% in the flow above the step. Transition to turbulence was not promoted artificially, neither in the experiment nor in the numerical simulation. In the initial phase of the numerical simulation transition is triggered via errors arising from the numerical solution method. However, during the major phase of the calculation (i.e. after the statistical steady-state has been reached) the transition in the free shear layer is induced via feedback of random three-dimensional fluctuations created in the re-attachment region. Immediately before the step the maximum magnitude of the stream-wise fluctuation intensity, u-rms, is of the order of 10^{-3}, whereas the lateral v-rms and the vertical w-rms are one order of magnitude smaller. However, immediately after the step the lateral v-rms exhibit values of the order of 10^{-3} to 10^{-2}, together with vertical fluctuations, w-rms, of the order of 10^{-3}. This indicates a 3D triggering of the separated laminar shear layer. In an additional DNS run with a forcing frequency of $St_h = 0.45$ and a very small forcing amplitude of $A = 10^{-5}$ no significant differences to the non-manipulated flow case were found for the second-order statistics.

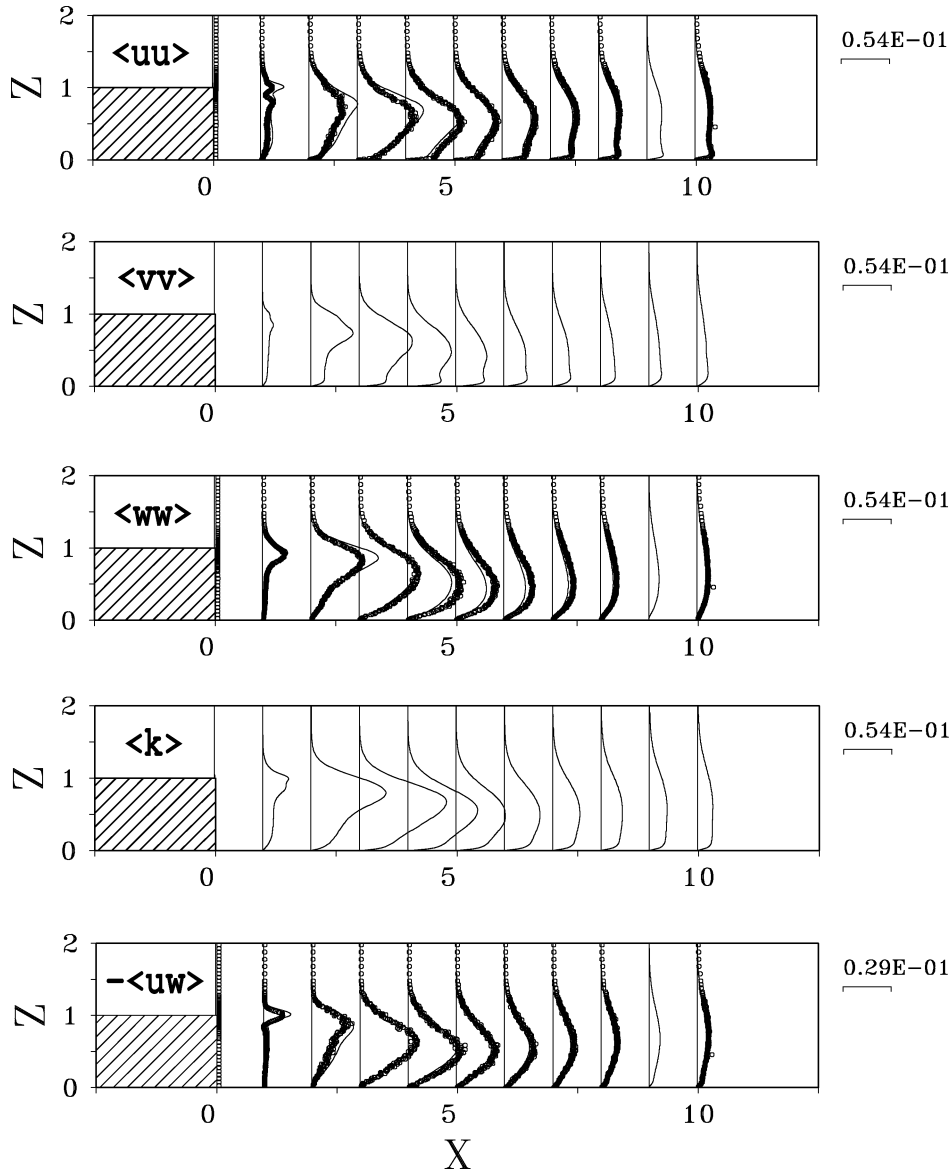

Figure 14. Vertical profiles of normal stresses $\langle uu \rangle$, $\langle vv \rangle$, $\langle ww \rangle$, and of turbulent kinetic energy $\langle k \rangle$ for the manipulated flow case at different positions X.

4.9. Using a higher-order numerical method

In numerical simulations of a 2D transitional boundary layer of Meri et al. [41] it has been demonstrated that a second-order numerical method needs about four times more grid points in comparison to a fourth-order Hermitian (or compact) method to produce correct amplification/damping rates in accordance with the linear stability theory. Therefore, the fully 3D and time dependent flow case of a transitional backward- facing step flow has been recalculated using a fourth-order (compact) discretization on the same computational grid as used with the second-order central differencing method. *Figure 3* shows that the u-rms profiles from second- and fourth-order calculations agree well with the hot-wire measurements at the edge of the step. In the transitional

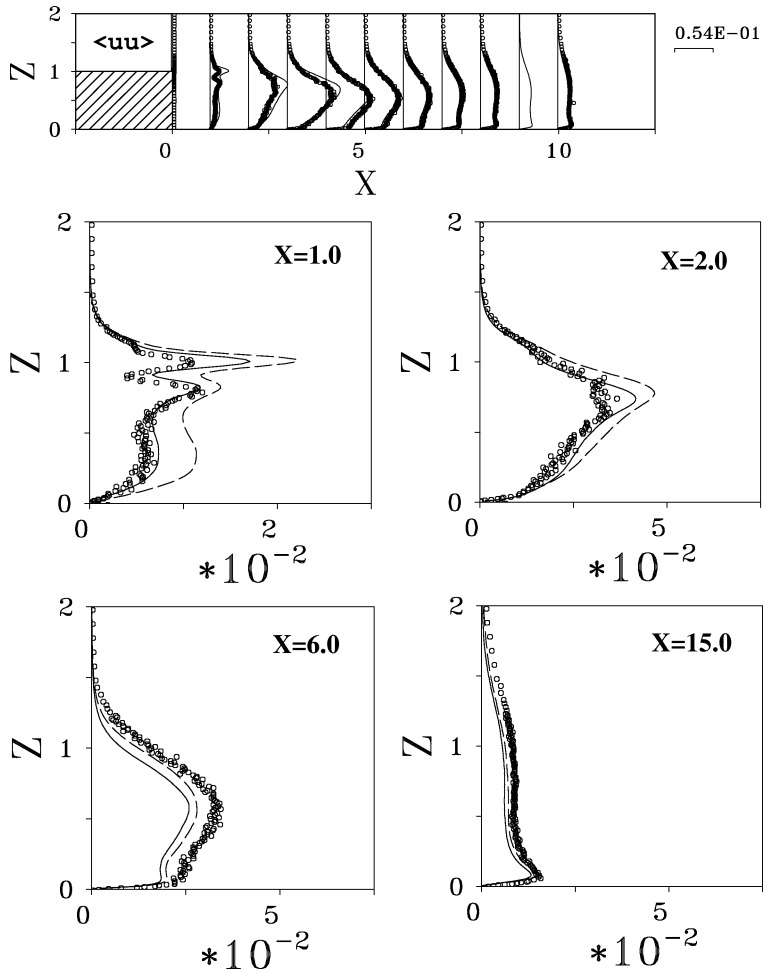

Figure 15. Vertical profiles of longitudinal normal stress $\langle uu \rangle$ for the manipulated flow case at different positions X: (dashed line) 2nd-order method, (full line) 4th-order (compact) method, (symbols) experiment.

regime after the step (see *figures 12*, *13* and *15*), the fourth-order results are quantitatively closer to the experimental data from LDA measurements. With increasing distance from the edge of the step the results from using either a second-order method or a fourth-order method are approaching each other continuously. The wall-skin friction coefficients (see *figure 10*) evaluated from second-order and fourth-order calculations agree very well with the experimental data. In general, the agreement of the fourth-order result is better for the manipulated case than for the non-manipulated case.

4.10. Instantaneous vorticity field

The most active flow regimes are the free shear layer undergoing transition to turbulence and the re-attachment zone. *Figure 17* shows four successive instantaneous flow states (in clockwise direction) during a full cycle (phase angle $\phi = 0$ to 2π) of the time-periodic (harmonic) 2D blowing/suction forcing at the edge of the step. The instantaneous span-wise vorticity contours (ω_y) show the large-scale roll-up of the shear layer

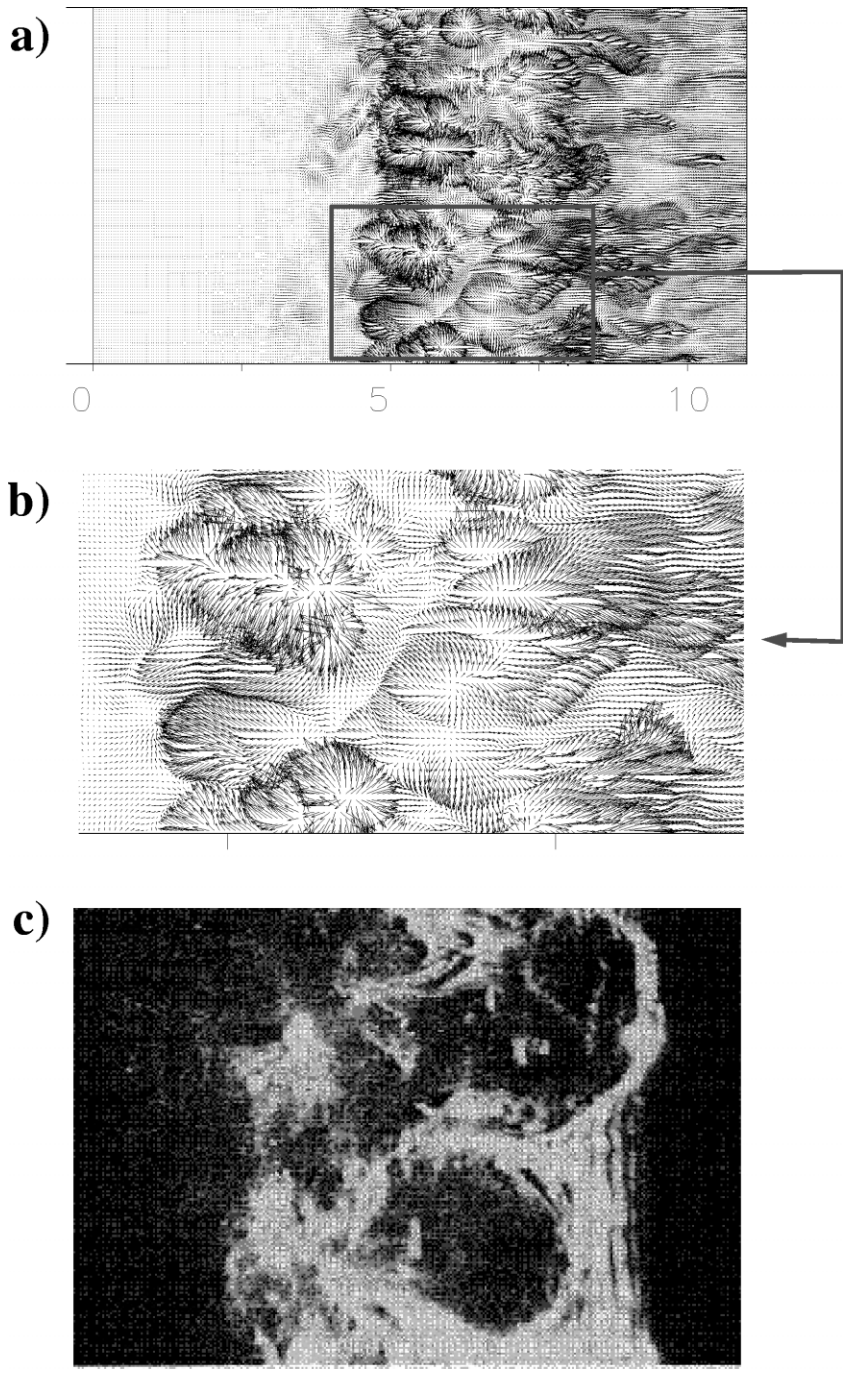

Figure 16. Flow structure in the re-attachment region (non-manipulated reference case) in a horizontal plane close to the wall ($Z = 0.008$): (a), (b): vector plot of instantaneous flow field; (c): visualization of flow around stagnation regions in reverse-flow regime [40].

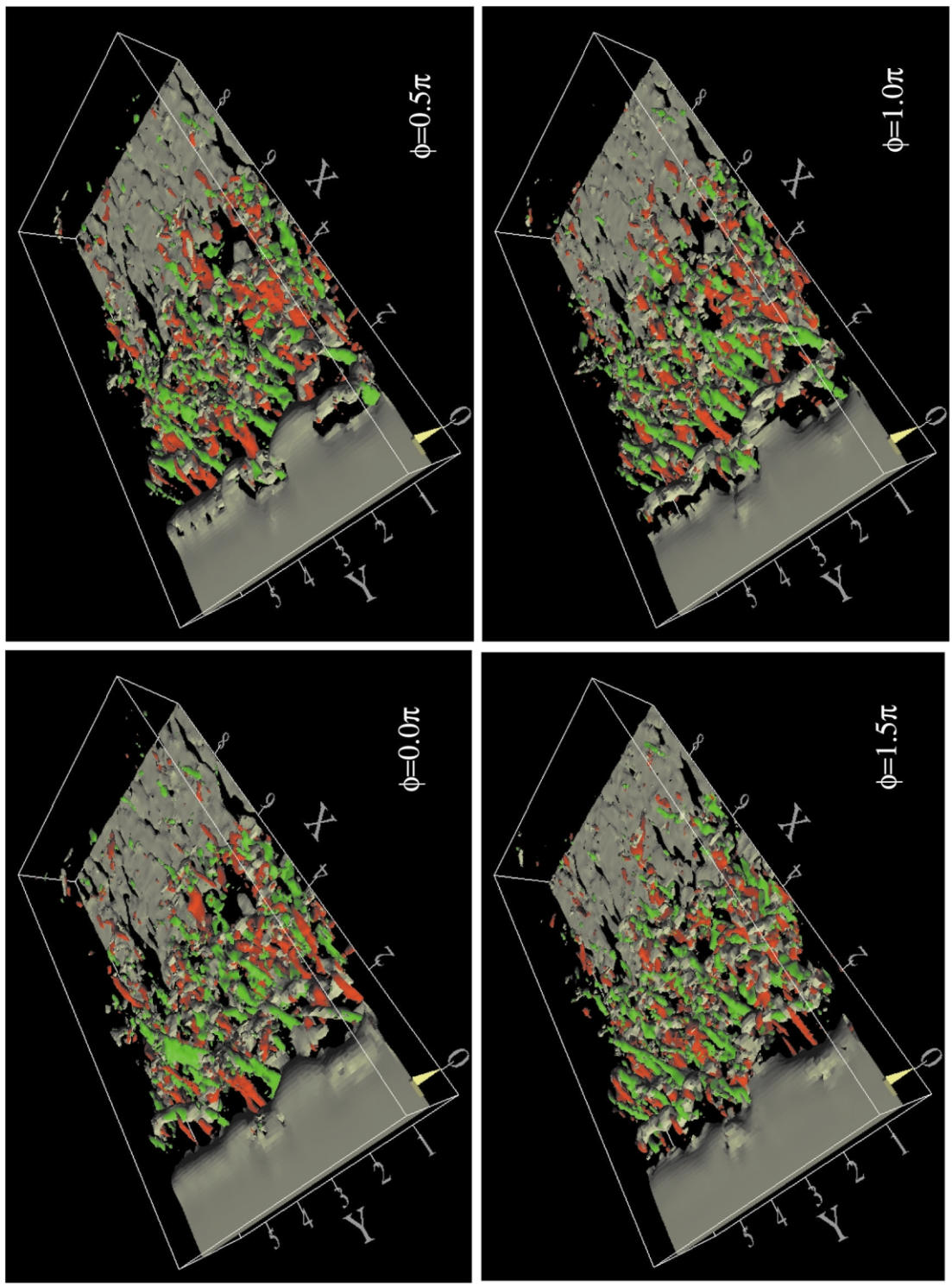

Figure 17. Instantaneous flow structure (manipulated case) at different phase angles ($\phi = 0, \pi/2, \pi, (3/2)\pi$) during a full cycle of the time-periodic forcing (with $St_h = 0.45$, $A = 0.01$). Surfaces of constant dimensionless vorticity: lateral vorticity $\omega_y = 5.0$ (gray), positive longitudinal vorticity $\omega_x = +4.0$ (green), negative longitudinal vorticity $\omega_x = -4.0$ (red).

and the creation of a lateral roller. This lateral roller exhibits some wavyness in the lateral direction, and the longitudinal vorticity (ω_x) (positive: green, negative: red) seems to be created preferably in the undulated parts.

5. Conclusions

An experimental and direct numerical simulation of a manipulated transitional backward-facing step flow showed that a significant reduction (33%) of the length of the mean reverse-flow region was obtained if the flow was manipulated by a low-amplitude time-periodic (harmonic) blowing/suction excitation through a narrow slot at the edge of the step. The forcing amplitude was of the order of one percent of the maximum inflow velocity. The optimum forcing frequency for a maximum reduction of the mean re- attachment length was around 50 Hz. The experimental data show that this is the most amplified frequency in the transition-to-turbulence process of the separated laminar shear layer. Increasing the ratio of momentum thickness to step height (from $\theta/h = 0.0266$ to $\theta/h = 0.0566$) by lowering the step height (from 20 mm to 10 mm) resulted in a maximum reduction of the mean re-attachment length at about the same forcing frequency, $f_{\text{opt}} \approx 50$ Hz. This leads to the conclusion that in our step flow case (with a small ratio θ/h) the optimum forcing frequency scales with the momentum thickness at the step and not with the step height. The corresponding optimum forcing Strouhal number is $St_\theta = f_{\text{opt}}\theta/U_o = 0.012$. The obvious effect of the forcing on the instantaneous flow field was that the downstream distance to the location of the first lateral roller in the free shear layer was significantly shortened. Increasing the forcing amplitude at the same forcing frequency resulted in an additional reduction of the mean re-attachment length.

The flow fields in the non-manipulated and manipulated flow cases are very complex showing a large-scale roll-up of the free shear layer, the creation of three-dimensional structures during the transition process, and one pairing process only was visible in the shear layer. There is a strong effect of the re-attachment on the transition via a feedback of 3D fluctuations. Strong velocity fluctuations parallel to the bottom wall are created around local stagnation flow patches at the end of the recirculation region close to the instantaneous re-attachment line. Finally, there is a very slow recovery (after the re-attachment zone) to a fully developed turbulent boundary layer (far outside of the computational domain).

Direct numerical simulation (DNS) is capable of predicting the experimental data qualitatively as well as quantitatively. Some remarks may however be helpful. Equivalent inflow conditions for the experiment and the DNS are very important. The largest quantitative differences between DNS and experimental data are observed in the dead-water zone close to the step with low turbulence intensities (low compared to the values in the re-attachment region). Applying a fourth-order compact numerical scheme improved the results in the transition region. However, in and downstream of the re-attachment zone, there are only small differences in the 2nd- and 4th-order simulation results for the second-order statistics.

The complementary nature of the experiment and the DNS became obvious during our joint experimental and numerical simulation investigation: in our case, the main advantage of the experiment was the relative easiness with which the optimal forcing frequency could be determined (with DNS a nearly impossible or at least a very expensive task). On the other hand, DNS is capable to provide spatio-temporal details of the flow which cannot be easily obtained in the experiment.

Acknowledgments

This research has been supported by the Deutsche Forschungsgemeinschaft (DFG) under grant number We 705/4+6, by a grant within a University Research Project, UF8 (Prof. H.H. Fernholz), at the Technical Univer-

sity of Berlin. We also gratefully acknowledge the support by the Konrad-Zuse-Zentrum für Informationstechnik Berlin (ZIB), in particular by K. Ketelson (from Silicon Graphics/Cray Research), the Leibniz Computing Center (LRZ) of the Bavarian Academy of Sciences, and the computing center of the Federal Armed Forces University Munich.

References

[1] Moin P., Mahesh K., Direct numerical simulation: a tool in turbulence research, Ann. Rev. Fluid Mech. 30 (1998) 539–5378.
[2] Eaton J.K., Johnston J.P., A review of research on subsonic turbulent flow reattachment, AIAA J. 19 (1981) 1093–1100.
[3] Adams E.W., Johnston J.P., Effects of the separating shear layer on the reattachment flow structure, part 1: pressure and turbulence quantities, Exp. Fluids 6 (1988) 400–408.
[4] Adams E.W., Johnston J.P., Effects of the separating shear layer on the reattachment flow structure, part 2: reattachment length and wall shear stress, Exp. Fluids 6 (1988) 493–499.
[5] Le H., Moin P., Kim J., Direct numerical simulation of turbulent flow over a backward-facing step, J. Fluid Mech. 330 (1997) 349–374.
[6] Akselvoll K., Moin P., Large eddy simulation of a backward facing step flow, in: Rodi W., Martelli F. (Eds.), Proceedings of Engineering Turbulence Modelling and Experiments 2, Elsevier Science, 1993, pp. 303–313.
[7] Jovic S., Driver D.M., Backward-facing step measurement at low Reynolds number, $Re = 5000$, NASA Tech. Mem. 108807, 1994.
[8] Delcayre F., Topology of coherent vortices in the reattachment region of a backward-facing step, Proc. 11th Symposium on Turbulent Shear Flows, September 8–10, Grenoble, France, 1997, pp. 26/24–29.
[9] Itoh N., Kasagi N., Turbulence measurement in a separated and reattaching flow over a backward-facing step with the three-dimensional particle tracking velocimeter (in Japanese), J. Flow Visualization Soc. Japan 34 (1989) 245.
[10] Kasagi N., Matsunaga A., Kawara S., Turbulence measurement in a separated and reattaching flow over a backward-facing step with the aid of three-dimensional particle tracking velocimetry, J. Wind Eng. Ind. Aerod. 46/47 (1993) 821–829.
[11] Nezu I., Nakagawa H., Turbulent structure of backward-facing step flow and coherent vortex shedding from reattachment in open channel flows, Turbulent Shear Flows 6 (1989) 314–337.
[12] Kobayashi T., Togashi S., Comparison of turbulence models applied to backward-facing step flow by LES data base, in: Rodi W., Martelli F. (Eds.), Proceedings of Engineering Turbulence Modelling and Experiments 2, Elsevier Science, 1993.
[13] Yoo J.Y., Baik S.J., Redeveloping turbulent boundary layer in the backward-facing step flow, J. Fluids Eng. 114 (1992) 522–529.
[14] Friedrich R., Arnal M., Turbulent backward-facing step flow, in: Gersten K. (Ed.), Physics of separated flows – numerical, experimental, and theoretical aspects, Notes on Numerical Fluid Mechanics, Vol. 40, Vieweg, 1993, pp. 7–17.
[15] Durst F., Schmitt F., Experimental study of high Reynolds number backward-facing step flow, Proc. 5th Symposium on Turbulent Shear Flows, August 7–9, Cornell U., Ithaca, NY, 1985.
[16] Sinha S.N., Gupta A.K., Oberai M.M., Laminar separating flow over backsteps and cavities, part 1: backsteps, AIAA J. 19 (1981) 1527–1530.
[17] Kaiktis L., Karniadakis G.E., Orszag S.A., Onset of three-dimensionality, equilibria, and early transition in flow over a backward-facing step, J. Fluid Mech. 231 (1991) 501–528.
[18] Neto A.S., Grand D., Metais O., Lesieur M., A numerical investigation of the coherent vortices in turbulence behind a backward-facing step, J. Fluid Mech. 256 (1993) 1–25.
[19] Bushnell D.M., McGinley C., Turbulence control in wall flows, Ann. Rev. Fluid Mech. 21 (1989) 1–20.
[20] Fiedler H.E., Fernholz H.H., On management and control of turbulent shear flows, Prog. Aerospace Sci. 27 (1990) 305–387.
[21] Gad-el Hak M., Interactive control of turbulent boundary layers: a futuristic look, AIAA J. 32 (1994) 1753–1765.
[22] Lumley J., Blossey P., Control of turbulence, Ann. Rev. Fluid Mech. 30 (1998) 311–327.
[23] Gad-el Hak M., Pollard A., Bonnet J.-P. (Eds.), Flow Control: Fundamentals and Practices, Lecture Notes in Physics, Vol. 53, Springer-Verlag, Berlin, 1998.
[24] Kiya M., Shimuzi M., Mochizuki O., Ido Y., The forced turbulent separation bubble, in: 9th Symp. Turbulent Shear Flows, August 16–18, 1993, Kyoto, Japan.
[25] Sigurdson L.W., The structure and control of a turbulent reattaching flow, J. Fluid Mech. 298 (1995) 139–165.
[26] Hasan M.A.Z., The flow over a backward-facing step under controlled disturbation: laminar separation, J. Fluid Mech. 238 (1992) 73–96.
[27] Hasan M.A.Z., Khan A.S., On the stability characteristics of a reattaching shear layer with nonlaminar separation, Int. J. Heat Fluid Flow 13 (1992) 224–231.
[28] Chun K.B., Sung H.J., Control of turbulent separated flow over a backward-facing step by local forcing, Exp. Fluids 21 (1996) 417–426.
[29] Chun K.B., Sung H.J., Response of separated flows over a backward-facing step to local forcing, 11th Symposium on Turbulent Shear Flows, September 8–11, Grenoble, France, 1997, pp. 26/13–26/17.
[30] Orellano A., Wengle H., Numerical simulation (DNS and LES) of manipulated turbulent boundary layer flow over a surface-mounted fence, Eur. J. Mech. B/Fluids 19 (5) (2000) 765–788.
[31] Bärwolff G., Wengle H., Jeggle H., Direct numerical simulation of transitional backward-facing step flow manipulated by oscillating blowing/suction, in: Rodi W., Bergeles G. (Eds.), Engineering Turbulence Modelling and Experiment 3, Elsevier Science, 1996, pp. 219–228.

[32] Huppertz A., Janke G., Preliminary experiments on the control of three-dimensional modes in the flow over a backward-facing step, in: Machiels L., Gavrilakis S., Monkewitz P.A. (Eds.), Advances in Turbulence VI, Kluwer Academic Publishers, 1996, pp. 461–464.
[33] Dengel P., Über die Struktur und Sensibilität einer inkompressiblen turbulenten Grenzschicht am Rande der Ablösung, PhD thesis, Technische Universität Berlin, 1992.
[34] Janke G., Über die Grundlagen und einige Anwendungen der Ölfilminterferometrie zur Messung von Wandreibungsfeldern in Luftströmungen, PhD thesis, Technische Universität Berlin, 1992.
[35] Mehta R.D., The aerodynamic design of blower tunnels with wide angle diffusors, Prog. Aerospace Sci. 18 (1977) 59–120.
[36] Bechert D.W., A model of the exitation of large fluctuations in a shear layer, AIAA paper No. 83-0724, 1983.
[37] Michalke A., Kozlov V.V., Dovgal A.V., Contribution to the instability of a laminar flow along axissymmetric bodies, part I: theory, Eur. J. Mech. B/Fluids 14 (1995) 333–350.
[38] Dovgal A.V., Kozlov V.V., Michalke A., Contribution to the instability of a laminar flow along axissymmetric bodies, part II: experiments and comparison with theory, Eur. J. Mech. B/Fluids 14 (1995) 351–365.
[39] Bradshaw P., The effect of initial conditions on the development of a free shear layer, J. Fluid Mech. 26 (1996) 225–236.
[40] Fernholz H.H., Near-wall phenomena in turbulent separated flows, Acta Mech. Suppl. 4 (1994) 57–67.
[41] Meri A., Wengle H., Dejoan A., Védy E., Schiestel R., Application of a 4th-order Hermitian scheme for non-equidistant grids to LES and DNS of incompressible fluid flow, in: Hirschel E.H. (Ed.), Numerical Flow Simulation I, Notes on Numerical Fluid Mechanics, Vol. 66, Vieweg, 1998, pp. 382–406.